A flexible piezoresistive pressure sensor based on PVA/GO/carboxylated carbon nanotube composite films

Yunzheng Zhang(张允政), Tao Wang(王涛), Wenjin Luo(骆文瑾), Sen Yang(杨森), Weiqi Zhu(朱伟琪), Shushu Chen(陈树澍), Liuhua Mu(木留华), Yan Fan(樊艳), Jie Jiang(江杰), Liang Chen(陈亮)
Citation: Chin. Phys. B. 35, 107303 (2026). DOI: 10.1088/1674-1056/ae9a5d | CSTR: 32038.14.CPB.ae9a5d
http://cpb.iphy.ac.cn; http://iopscience.iop.org/cpb

What follows is a list of articles you may be interested in

An enhanced MXene/LIG composite structure-based flexible sensor for real-time pilot motion monitoring

Mian Zhong(钟勉), Hongyun Fan(范红云), Zhanghui Wu(吴章辉), Xiaoqing Xing(邢晓晴), Yilin Zhao(赵一霖), Lin Li(李麟), Yong Jiang(蒋勇), Qinglei Li(李庆磊), Kaixin Xu(徐开心), Kun Luo(罗鲲), Guogang Ren(任国刚), Jie Wu(吴杰)
Chin. Phys. B. 35, 058102 (2026). DOI: 10.1088/1674-1056/ae32fe | CSTR: 32038.14.CPB.ae32fe

Adsorption dynamics of double-stranded DNA on a graphene oxide surface with both large unoxidized and oxidized regions

Mengjiao Wu(吴梦娇), Huishu Ma(马慧姝), Haiping Fang(方海平), Li Yang(阳丽), Xiaoling Lei(雷晓玲)
Chin. Phys. B. 32, 018701 (2023). DOI: 10.1088/1674-1056/ac5c3a

Highly stable two-dimensional graphene oxide: Electronic properties of its periodic structure and optical properties of its nanostructures

Qin Zhang(张琴), Hong Zhang(张红), Xin-Lu Cheng(程新路)
Chin. Phys. B. 27, 027301 (2018). DOI: 10.1088/1674-1056/27/2/027301

Frequency and voltage-dependent electrical and dielectric properties of Al/Co-doped PVA/p-Si structures at room temperature

Ibrahim Yücedağ, Ahmet Kaya, Şemsettin Altındal, Ibrahim Uslu
Chin. Phys. B. 23, 047304 (2014). DOI: 10.1088/1674-1056/23/4/047304

SPECIAL TOPIC — A 40th Anniversary Celebration: Physics Research and Innovation at Ningbo University

A flexible piezoresistive pressure sensor based on PVA/GO/carboxylated carbon nanotube composite films

Yunzheng Zhang(张允政)[1,†], Tao Wang(王涛)[1,†], Wenjin Luo(骆文瑾)[3], Sen Yang(杨森)[2], Weiqi Zhu(朱伟琪)[3], Shushu Chen(陈树澍)[1], Liuhua Mu(木留华)[1], Yan Fan(樊艳)[2,‡], Jie Jiang(江杰)[1,§], and Liang Chen(陈亮)[1]

[1] *School of Physical Science and Technology, Ningbo University, Ningbo* 315211, *China*
[2] *College of Optical, Mechanical and Electrical Engineering, Zhejiang A&F University, Hangzhou* 311300, *China*
[3] *College of Physics Science and Technology, Yangzhou University, Yangzhou* 225009, *China*

(Received 31 May 2026; revised manuscript received 6 August 2026; accepted manuscript online 17 August 2026)

Flexible piezoresistive pressure sensors hold great promise for wearable health monitoring, motion recognition, and human–machine interaction. However, achieving high sensitivity, a broad pressure-response range, and long-term operational stability in composite-film-based devices remains challenging. Herein, we report a flexible piezoresistive pressure sensor based on a poly(vinyl alcohol) (PVA)/graphene oxide (GO)/carboxyl-functionalized carbon nanotube (COOH-CNT) composite film. The sensing film was fabricated by blade coating a homogeneous PVA/GO/COOH-CNT aqueous ink, followed by thermal drying at 60 °C for 24 h, and the device was assembled into a sandwich structure using Pt/PI electrodes. The composite film exhibited a continuous layered morphology, in which GO sheets provided a lamellar framework and COOH-CNTs acted as conductive bridges for pressure-induced resistance modulation. The sensor exhibited approximately linear current–voltage characteristics over the voltage range from −2 V to 2 V under applied pressures ranging from 0 to 88.4 kPa, with coefficients of determination (R^2) ranging from 0.98527 to 0.99289. The normalized current response exhibited three sensitivity regimes, with sensitivities of 152.1 kPa^{-1}, 39.7 kPa^{-1}, and 14.5 kPa^{-1} over the pressure ranges of 44.2 Pa–8.49 kPa, 8.49–84.07 kPa, and 84.07–309.73 kPa, respectively. The device achieved a low detection limit of 44.2 Pa, a broad pressure-response capability up to 397.89 kPa, and response/recovery times of 333 ms and 267 ms, respectively, determined using the 90% signal-change criterion. Moreover, stable output was maintained over more than 5000 loading–unloading cycles at approximately 4.42 kPa. Wearable demonstrations, including wrist-pulse monitoring, finger and wrist bending detection, and respiration monitoring, confirmed the capability of the sensor to detect both subtle physiological signals and large-amplitude human motions. This work provides a facile strategy for developing flexible composite-film pressure sensors for wearable sensing applications.

Keywords: flexible pressure sensor, piezoresistive, PVA, graphene oxide, carboxylated carbon nanotubes, wearable monitoring.

PACS: 73.61.–r, 72.80.Tm, 85.40.Ls, 68.35.bg

DOI: 10.1088/1674-1056/ae9a5d **CSTR:** 32038.14.CPB.ae9a5d

1. Introduction

Flexible pressure sensors have attracted extensive attention in recent years owing to their promising applications in wearable health monitoring, electronic skin, soft robotics, tactile sensing, and human–machine interaction.[1–7] Unlike conventional rigid pressure sensors, flexible pressure sensors can conformally attach to curved or deformable surfaces and convert external mechanical stimuli into readable electrical signals, enabling real-time detection of human motions and physiological signals such as joint bending, respiration, pulse waves, and tactile pressure. According to their signal-transduction mechanisms, flexible pressure sensors can generally be classified into piezoresistive, capacitive, piezoelectric, and triboelectric types.[8–10] Among them, piezoresistive sensors are particularly attractive because of their simple device configuration, convenient electrical readout, low power consumption, and facile integration with flexible electronic systems.[11,12]

For piezoresistive pressure sensors, the sensing performance is mainly determined by pressure-induced resistance variation in the active sensing layer. In conductive polymer composites, external compression can modulate the internal conductive network by increasing effective conductive contacts, shortening the distance between conductive fillers, facilitating electron transport, and reducing interfacial contact resistance.[13,14] These changes lead to a measurable resistance decrease or current increase under an applied bias voltage. Although considerable progress has been achieved, it remains challenging to simultaneously realize high sensitivity, a broad pressure-response range, a low detection limit,

[†]These authors contributed equally to this work
[‡]Corresponding author. E-mail: fanyan503@zafu.edu.cn
[§]Corresponding author. E-mail: jiangjie1@nbu.edu.cn

© 2026 Chinese Physical Society and IOP Publishing Ltd. All rights, including for text and data mining, AI training, and similar technologies, are reserved.

fast response/recovery, and long-term stability.[15] Highly deformable microstructured sensors often show high sensitivity at low pressure but may suffer from a limited working range or signal saturation at higher pressure. Meanwhile, irreversible rearrangement of conductive fillers, viscoelastic deformation of polymer matrices, and environmental interference may cause hysteresis, baseline drift, and poor cyclic durability.[16–20]

Material selection and structural design are therefore critical for improving the comprehensive performance of flexible piezoresistive sensors. Carbon-based and two-dimensional nanomaterials, including graphene, graphene oxide (GO), reduced graphene oxide, carbon nanotubes (CNTs), and MXene-based materials, have been widely investigated because of their high aspect ratio, tunable surface chemistry, and ability to construct pressure-sensitive conductive networks.[21–24] Two-dimensional graphene-based sheets can provide large interfacial contact areas and layered frameworks, while one-dimensional CNTs can serve as conductive bridges between adjacent domains, facilitating charge transport and improving network connectivity.[25,26] Compared with pristine carbon nanomaterials, functionalized nanocarbon materials are more suitable for solution processing and polymer-composite fabrication because their surface functional groups can improve dispersion stability and interfacial compatibility. In particular, carboxyl-functionalized carbon nanotubes (COOH-CNTs) possess abundant carboxyl groups, which can enhance their dispersibility in aqueous systems and promote interactions with other functional components.[27]

Poly(vinyl alcohol) (PVA) is a promising polymer matrix for flexible composite sensing films because of its water processability, good film-forming ability, flexibility, and abundant hydroxyl groups. These hydroxyl groups can interact with oxygen-containing groups on GO and carboxyl groups on COOH-CNTs, which is beneficial for homogeneous filler dispersion and stable interfacial interactions. Previous studies have shown that PVA/GO composite films and PVA/CNT-based systems can exhibit mechanical flexibility and pressure-responsive behavior under external stimuli.[28] However, many reported flexible pressure sensors rely on porous templates, electrospinning, dip coating, or relatively complex structural engineering. Developing a simple, solution-processable composite film with a stable microstructure, effective conductive pathways, and reliable pressure-sensing performance remains desirable. Ink-based printing and coating strategies have also been widely explored for scalable fabrication of flexible functional devices, highlighting the advantages of solution-processable material systems.[29–31]

Recent studies have demonstrated that the comprehensive performance of flexible piezoresistive pressure sensors can be improved through coordinated regulation of material interfaces, conductive networks, and deformable structures. For example, Gu *et al.*[32] developed a pressure sensor using a nested-cell architecture and molecular surface modification, demonstrating that multiscale structural design can combine high sensitivity with a broad pressure range. Hu *et al.*[33] developed a CTS/CNTs-OH composite-fabric pressure sensor by combining functionalized carbon nanotubes with textile-layer engineering, highlighting the roles of conductive-network regulation and multilayer interfacial contact in sensing linearity, stability, and human-motion recognition. These studies show that rational control of interfaces and pressure-dependent conductive pathways is important for balanced sensing performance. In contrast, the present work focuses on a compact PVA/GO/COOH-CNT composite film fabricated through a facile aqueous solution-processing and blade-coating strategy.

Herein, we report a flexible piezoresistive pressure sensor based on a PVA/GO/COOH-CNT composite film. The composite sensing film was fabricated through an aqueous solution-processing and blade-coating method, followed by thermal drying. In this design, PVA serves as the flexible film-forming matrix, GO sheets provide a layered structural framework, and COOH-CNTs act as conductive bridges for pressure-induced resistance modulation. The assembled sandwich-structured sensor exhibited approximately linear current–voltage characteristics from -2 V to 2 V under applied pressures from 0 to 88.4 kPa, with R^2 values of 0.98527–0.99289, together with a low detection limit of 44.2 Pa, a broad pressure-response capability up to 397.89 kPa, response/recovery times of 333 ms and 267 ms, and stable output over more than 5000 loading–unloading cycles at approximately 4.42 kPa. Wearable demonstrations, including wrist-pulse monitoring, finger bending, wrist bending, and respiration monitoring, confirmed the capability of the sensor to detect both subtle physiological signals and large-amplitude human motions. This work provides a facile route for constructing flexible PVA/GO/COOH-CNT composite-film pressure sensors for wearable sensing applications.

2. Experimental details

2.1. Materials

Graphite powder (8000 mesh), sulfuric acid (H_2SO_4), potassium persulfate ($K_2S_2O_8$), phosphorus pentoxide (P_2O_5), potassium permanganate ($KMnO_4$), hydrogen peroxide (H_2O_2), hydrochloric acid (HCl), PVA, and COOH-CNTs were purchased from Shanghai Aladdin Bio-Chem Technology Co., Ltd. and used as received unless otherwise stated. The PVA had a viscosity of 3.5–4.5 mPa·s for a 4% aqueous solution and a polymerization degree of approximately 200–300. The COOH-CNTs possessed a purity higher than

99%, an inner diameter of 3–5 nm, an outer diameter of 8–15 nm, a length of 5–15 μm, and a carboxyl group content of 1 mmol·g^{-1}. High-purity deionized water with a resistivity of 18.2 MΩ·cm was used throughout the experiments.

2.2. Preparation of GO dispersion

GO suspension was prepared from graphite powder according to a previously reported modified Hummers' method. Briefly, graphite powder was added into a mixed solution containing H_2SO_4, $K_2S_2O_8$, and P_2O_5 for pre-oxidation. The mixture was continuously stirred for 4.5 h. After the reaction, the product was washed with deionized (DI) water and collected by centrifugation to remove residual acids and impurities. The pre-oxidized graphite was then obtained by vacuum drying at 60 °C. Subsequently, the pre-oxidized graphite was further oxidized in a concentrated sulfuric acid medium under an ice bath, during which $KMnO_4$ was added gradually to control the reaction. After oxidation, the mixture was diluted with DI water, followed by the addition of 30 wt% H_2O_2 solution to terminate the reaction. The resulting product was washed with an aqueous HCl solution (HCl:H_2O = 1:10) and collected by centrifugation to remove metal ions and other impurities, and then repeatedly washed with DI water. For further purification, the obtained GO dispersion was dialyzed using a dialysis membrane (dialysis bag) with a volume ratio of GO dispersion to ultrapure water of 1:100 (GO: ultrapure water = 1:100). The external ultrapure water was replaced continuously until the conductivity of the GO dispersion approached ∼ 1 μS·cm^{-1}. Finally, the product was diluted to 1 L with DI water and sonicated to promote exfoliation and uniform dispersion, yielding a GO suspension with a concentration of approximately 5 mg·mL^{-1}.

2.3. Preparation of PVA/GO/COOH-CNT mixed ink and film fabrication

The preparation process of the PVA/GO/COOH-CNT composite sensing film is schematically illustrated in Fig. 1(a). First, 0.02 g of COOH-CNTs was added into 10 mL of GO aqueous dispersion with a concentration of 5 mg·mL^{-1}. The mixture was then ultrasonicated for 20 min to promote the uniform dispersion of COOH-CNTs in the GO suspension and to obtain a stable GO/COOH-CNT mixed dispersion.

Separately, a 1.0 wt% PVA aqueous solution was prepared by dissolving PVA in deionized water under magnetic stirring at 90 °C for 4 h until a transparent and homogeneous solution was obtained. Subsequently, 0.4 mL of the PVA solution was added into the GO/COOH-CNT dispersion and stirred at 25 °C for 2 h to form a uniform PVA/GO/COOH-CNT composite ink. The introduction of PVA improved the film-forming ability of the composite system, while the hydroxyl groups of PVA could interact with the oxygen-containing groups on GO and the carboxyl groups on COOH-CNTs, contributing to the dispersion stability and interfacial compatibility of the ink.

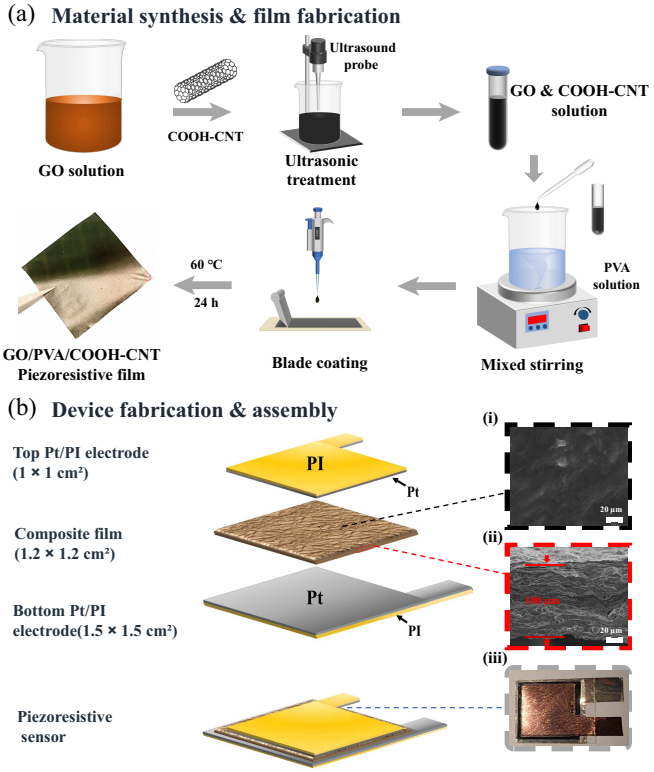

Fig. 1. Schematic illustration of the fabrication process, device assembly, and structural characterization of the PVA/GO/COOH-CNT flexible piezoresistive pressure sensor. (a) Preparation of the PVA/GO/COOH-CNT composite ink and piezoresistive film through dispersion of COOH-CNTs in GO solution, ultrasonication, mixing with PVA solution, blade coating, and thermal drying at 60 °C for 24 h. (b) Assembly of the sandwich-structured pressure sensor using a top Pt/PI electrode, PVA/GO/COOH-CNT composite film, and bottom Pt/PI electrode. Insets show (i) the surface scanning electron microscopy (SEM) image of the composite film, (ii) the cross-sectional SEM image showing a layered structure with a thickness of approximately 100 μm, and (iii) a photograph of the assembled flexible sensor.

For film fabrication, a Pt-coated polyimide (PI) substrate was fixed using PI tape, and a recessed square coating area of 1.5 × 1.5 cm^2 was defined. For each coating cycle, 100 μL of the PVA/GO/COOH-CNT composite ink was deposited within the defined area and manually spread by the same operator using a blade. Because a gap-controlled automatic film applicator was not used, the instantaneous blade speed and wet-film thickness of each coating layer were not instrumentally controlled. The deposited layer was dried at 60 °C for 30 min before the next coating cycle, and the coating–drying procedure was repeated five times. The coated film was then dried at 60 °C for 24 h to remove residual water. Process consistency was maintained by fixing the ink volume, coating area, operator, coating sequence, and drying conditions. The resulting five-cycle film had a final dry thickness of approximately 100 μm, as determined from the cross-sectional SEM image.

2.4. Device assembly

The flexible piezoresistive pressure sensor was assembled using the PVA/GO/COOH-CNT composite film as the active sensing layer and Pt-coated polyimide (Pt/PI) films as the electrodes, as schematically shown in Fig. 1(b). The PI substrate had a thickness of 200 μm. Pt layers were deposited onto commercial PI films by magnetron sputtering for 5 min to obtain flexible conductive electrodes with good electrical conductivity and mechanical compliance.

For device assembly, the PVA/GO/COOH-CNT composite sensing film was prepared with an active area of approximately 1.2×1.2 cm^2. Two Pt/PI electrodes were used as the bottom and top electrodes, with sizes of 1.5×1.5 cm^2 and 1.0×1.0 cm^2, respectively. The composite film was placed between the two Pt/PI electrodes to form a sandwich-structured flexible pressure sensor. The electrode lead regions were retained for connection to external electrical testing equipment. A photograph of the assembled flexible sensor is shown in Fig. 1(b)(iii), indicating the successful integration of the composite sensing film with the flexible Pt/PI electrodes.

In this configuration, the PVA/GO/COOH-CNT composite film served as the pressure-sensitive resistor, while the Pt/PI electrodes enabled current collection during loading and unloading. When external pressure was applied normal to the device surface, the internal conductive pathways of the composite film were modulated, resulting in a measurable resistance variation and a corresponding current response under a constant bias voltage.

3. Results and discussion

3.1. Working principle of the piezoresistive sensor

The PVA/GO/COOH-CNT composite-film sensor was operated in a constant-voltage mode, in which the output signal increased with increasing applied pressure, indicating a pressure-induced decrease in electrical resistance. For polymer-based conductive composites, the piezoresistive response mainly originates from the pressure-induced evolution of conductive pathways and micro-contact interfaces.[34,35] External compression can increase the number of effective conductive contacts, shorten the distance between conductive components, facilitate electron transport, and reduce interfacial contact resistance, thereby leading to a higher output current under pressure.[32,33]

In the PVA/GO/COOH-CNT composite film, PVA serves as the flexible matrix and film-forming component, GO sheets provide a layered structural framework, and COOH-CNTs act as conductive bridges between adjacent GO-rich domains.[9] This structure enables the formation of pressure-sensitive conductive pathways within the composite film. Under applied pressure, the elastic deformation of the PVA matrix promotes closer packing of the layered structure and increases the contact probability between conductive components, resulting in a reversible resistance variation. In addition, the hydroxyl groups of PVA can interact with the oxygen-containing groups of GO and the carboxyl groups of COOH-CNTs, which improves filler dispersion and interfacial compatibility. These interactions help stabilize the conductive network and suppress irreversible rearrangement during repeated compression and release, contributing to stable and repeatable piezoresistive sensing behavior.

Component-control experiments were performed to clarify the roles of PVA, GO, and COOH-CNTs (Supplementary Fig. S1). The PVA/GO film showed only weak and irregular pressure-dependent current variations, whereas the GO/COOH-CNT film exhibited distinguishable but relatively slow response and recovery. The PVA/COOH-CNT film had a low resistance of approximately 300 Ω and showed no resolvable pressure-dependent modulation under the investigated conditions, indicating the formation of a highly interconnected CNT network. In comparison, the ternary PVA/GO/COOH-CNT film exhibited clearer pressure discrimination and faster stabilization. These results support complementary roles of COOH-CNTs as the principal conductive pathways, GO as a regulator of conductive-network connectivity and interfacial contacts, and PVA as the film-forming and mechanically compliant matrix.

The influence of COOH-CNT content on the electrical response was further investigated using composite films containing 0, 20 mg, and 40 mg of COOH-CNTs (Supplementary Fig. S2). Without COOH-CNTs, the film exhibited only weak and non-monotonic current variations, indicating insufficient conductive-network connectivity. Increasing the COOH-CNT content to 20 mg produced clearly distinguishable pressure-dependent responses. At 40 mg, the current increased substantially, indicating a more highly connected conductive network; however, the differentiation among pressure levels became less pronounced relative to the baseline current. These results suggest that excessive COOH-CNT loading reduces the relative pressure-induced modulation of the conductive network. Among the investigated formulations, the 20 mg sample provided the best balance between electrical conduction and pressure-dependent response.

3.2. Microstructure of the composite film

The microstructure of the PVA/GO/COOH-CNT composite film was characterized by scanning electron microscopy, as shown in Figs. 1(b)(i) and 1(b)(ii). The surface SEM image in Fig. 1(b)(i) shows a continuous and compact film morphology without obvious large cracks or severe defects. Wrinkled sheet-like features can be observed on the film surface, which are associated with the assembly of GO sheets in the PVA matrix. Meanwhile, fine curved features

are distributed within the surface morphology, suggesting that COOH-CNTs are embedded in the composite network. Such a relatively uniform and continuous morphology is beneficial for maintaining stable electrical conduction and reducing signal fluctuation during pressure sensing.

The cross-sectional SEM image in Fig. 1(b)(ii) reveals a compact layered structure with a thickness of approximately 100 μm. The stacked lamellar morphology indicates that GO sheets form a layered framework after blade coating and thermal drying. COOH-CNTs can bridge adjacent layered domains, improving the connectivity of the conductive network. Upon external compression, the interlayer spacing and interfacial gaps decrease, additional conductive contacts are generated, and the contact resistance is reduced, giving rise to the piezoresistive response. Figure 1(b)(iii) further shows the assembled flexible sensor, demonstrating the feasibility of integrating the composite sensing film with Pt/PI electrodes into a sandwich-structured device. The continuous surface morphology, compact layered cross-section, and flexible device structure provide an important structural basis for the pressure-induced resistance variation of the PVA/GO/COOH-CNT composite-film sensor. These microstructural features support the sensing performance discussed in the following sections.

The influence of sensing-layer thickness was further evaluated by varying the number of coating–drying cycles while keeping the ink volume per cycle, coating area, and drying procedure unchanged (Supplementary Fig. S3). The number of coating cycles was used as an indicator of relative film thickness because the exact dry thicknesses of the three- and seven-cycle films were not directly measured; the five-cycle film had a cross-sectional thickness of approximately 100 μm. The three- and five-cycle films exhibited clearly distinguishable pressure-dependent responses, with the five-cycle film showing more stable cyclic signals. Increasing the number of coating cycles to seven reduced the pressure-dependent current modulation. Among the investigated conditions, five coating cycles provided the best balance between response magnitude, pressure discrimination, and cyclic stability.

3.3. Piezoresistive sensing performance

The piezoresistive sensing performance of the PVA/GO/COOH-CNT composite-film sensor was systematically investigated under external pressure, as shown in Fig. 2. Figure 2(a) illustrates the pressure-sensing measurement setup. During the measurement, the sensor was connected to an electrochemical analyzer for real-time electrical signal acquisition, while a Mark-10 force testing system was used to apply controlled pressure through a flat-ended cylindrical probe. The radius of the flat probe was 0.6 cm, and the applied pressure was calculated according to $P = F/A$, where F is the applied force and $A = \pi r^2$ is the contact area of the probe. The output signal was recorded to evaluate the pressure-dependent resistance variation of the composite sensing layer.

The electrical characteristics of the sensor under different pressures were first examined by voltage-sweep measurements. As shown in Fig. 2(b), the sensor exhibited approximately linear and nearly symmetric current–voltage characteristics over the voltage range from −2 V to 2 V under applied pressures ranging from 0 to 88.4 kPa. Linear fitting of the I–V curves yielded coefficients of determination (R^2) ranging from 0.98527 to 0.99289, indicating approximately ohmic electrical behavior and stable electrical contact within the investigated voltage range. Moreover, the slopes of the I–V curves gradually increased with increasing applied pressure, corresponding to enhanced electrical conductance and reduced device resistance. This pressure-dependent electrical behavior confirms that the sensing signal originates from resistance modulation of the PVA/GO/COOH-CNT composite film. Under compression, the interlayer spacing and filler–filler distance decrease, additional conductive contacts form, and the contact resistance is reduced, resulting in an increased output response. The pressure-dependent normalized response and sensitivity are shown in Fig. 2(c). The normalized current response was defined as

$$\Delta I/I_0 = (I - I_0)/I_0,$$

where I_0 is the initial current without applied pressure and I is the current under applied pressure. The sensitivity was calculated from the slope of the normalized response–pressure curve

$$S = \delta(\Delta I/I_0)/\delta P,$$

where P is the applied pressure. The response curve shows a segmented behavior with different sensitivities in different pressure regions. The corresponding sensitivities are 152.1 kPa^{-1} in the low-pressure region, 39.7 kPa^{-1} in the medium-pressure region, and 14.5 kPa^{-1} in the high-pressure region. The high sensitivity in the low-pressure region can be attributed to the rapid increase in effective conductive contacts and the shortened interfacial distance at the initial stage of compression. As the pressure further increases, the conductive network becomes gradually compacted, and the incremental change in newly formed conductive pathways decreases, leading to a reduced sensitivity in the medium- and high-pressure regions.

The pressure-response capability over a wide range was further evaluated, as shown in Fig. 2(d). The sensor exhibits clear stepwise output signals under different applied pressures from 1.77 kPa to 397.89 kPa. The output response increases with increasing pressure, and the signals remain distinguishable at different pressure levels. This result indicates that the composite-film sensor can maintain reliable pressure-responsive behavior over a broad pressure range. The clear and

repeatable stepwise responses also suggest reversible modulation of the conductive network during repeated loading and unloading.

The response and recovery characteristics of the sensor were evaluated under a pressure of approximately 50 kPa, as shown in Fig. 2(e). The response time was defined as the time required for the output signal to reach 90% of its total increase after loading, while the recovery time was defined as the time required for the signal to recover by 90% after unloading. Based on this 90% signal-change criterion, the response and recovery times were determined to be 333 ms and 267 ms, respectively. These results indicate that the conductive pathways in the PVA/GO/COOH-CNT composite film can be rapidly reconstructed under applied pressure and restored after pressure release, enabling real-time pressure-sensing capability.

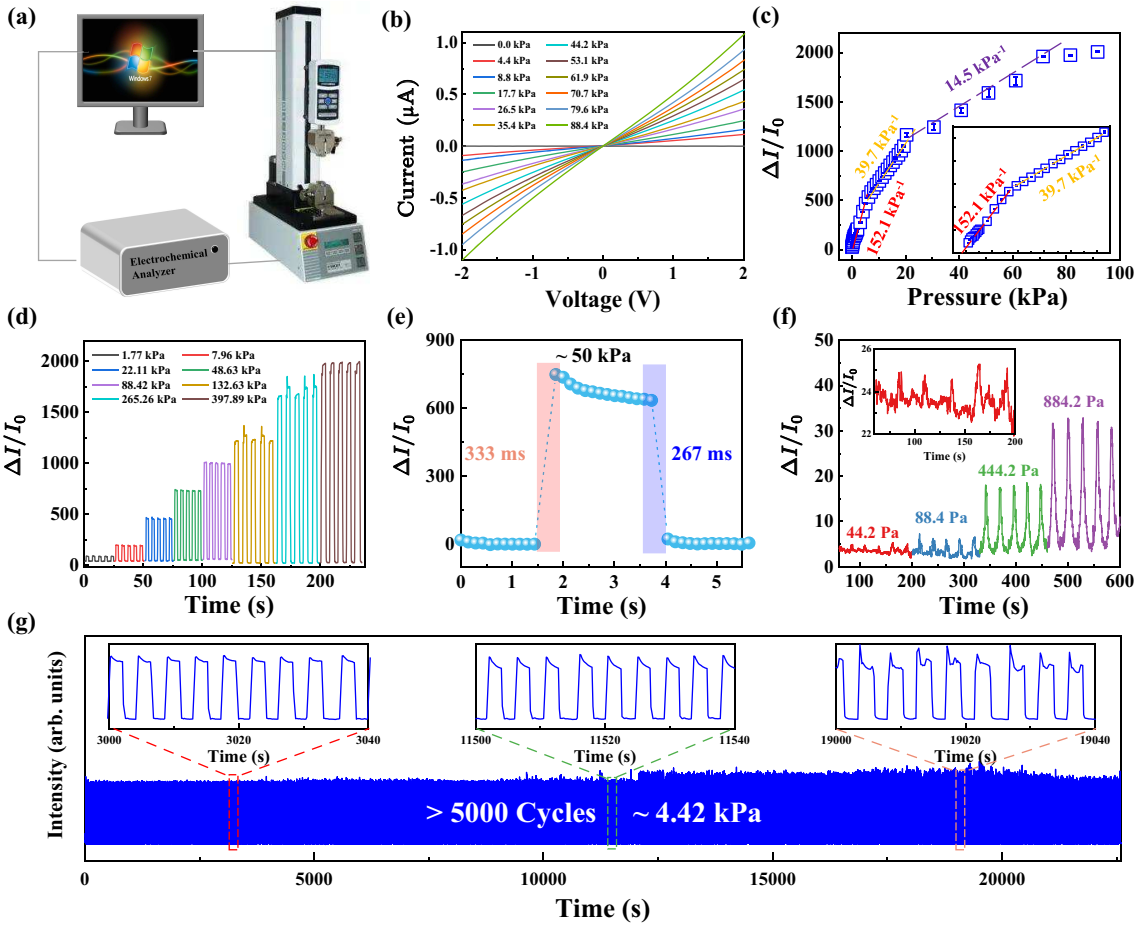

Fig. 2. Piezoresistive sensing performance of the PVA/GO/COOH-CNT composite-film sensor. (a) Schematic illustration of the pressure-sensing measurement setup using an electrochemical analyzer and a Mark-10 force testing system. (b) Current–voltage characteristics of the sensor measured over the voltage range from −2 V to 2 V under applied pressures ranging from 0 to 88.4 kPa. (c) Pressure-dependent normalized response and segmented sensitivity of the sensor, showing sensitivities of 152.1 kPa^{-1}, 39.7 kPa^{-1}, and 14.5 kPa^{-1} in different pressure regions. (d) Stepwise current responses of the sensor under different applied pressures from 1.77 kPa to 397.89 kPa. (e) Response and recovery behavior of the sensor under approximately 50 kPa, showing response and recovery times of 333 ms and 267 ms, respectively, determined using the 90% signal-change criterion. (f) Low-pressure responses of the sensor under pressures of 44.2 Pa, 88.4 Pa, 442.1 Pa, and 884.2 Pa. (g) Long-term cyclic stability of the sensor under repeated loading–unloading cycles at approximately 4.42 kPa for more than 5000 cycles.

The low-pressure detection capability of the sensor was investigated using weak pressure stimuli, as shown in Fig. 2(f). The device produced distinguishable responses under pressures of 44.2 Pa, 88.4 Pa, 442.1 Pa, and 884.2 Pa. Notably, the sensor could detect a pressure as low as 44.2 Pa, demonstrating its ability to respond to weak mechanical stimuli. The enlarged inset further confirms that the signal at 44.2 Pa can be clearly distinguished from the baseline fluctuation, indicating good low-pressure detectability. This behavior is attributed to the pressure-sensitive layered structure of the composite film, in which slight compression can effectively modulate conductive pathways and interfacial contact states.

Long-term cyclic stability was further examined by repeated loading–unloading tests at approximately 4.42 kPa. As shown in Fig. 2(g), the sensor maintains stable output over more than 5000 cycles, and no obvious signal failure is observed during the cyclic test. The enlarged signals at selected cycle regions show retained waveform characteristics, indicating good repeatability and mechanical durability of the sensing layer. This stability can be attributed to the continuous film morphology, the flexible PVA matrix, and the GO/COOH-CNT-assisted conductive network, which together help main-

tain reversible conductive-pathway evolution during repeated compression and release. These results demonstrate that the PVA/GO/COOH-CNT composite-film sensor possesses near-ohmic electrical behavior, segmented high sensitivity, broad pressure-response capability, low-pressure detectability, fast response/recovery characteristics, and reliable cyclic durability. These sensing features provide a solid basis for its application in wearable pressure sensing and human-signal monitoring.

4. Dynamic response and environmental adaptability

The dynamic response and environmental adaptability of the PVA/GO/COOH-CNT composite-film sensor were further investigated, as shown in Fig. 3. For wearable pressure sensors, reliable operation under different mechanical loading rates and ambient conditions is essential because practical human activities often involve variable deformation speeds, temperatures, and humidity levels.

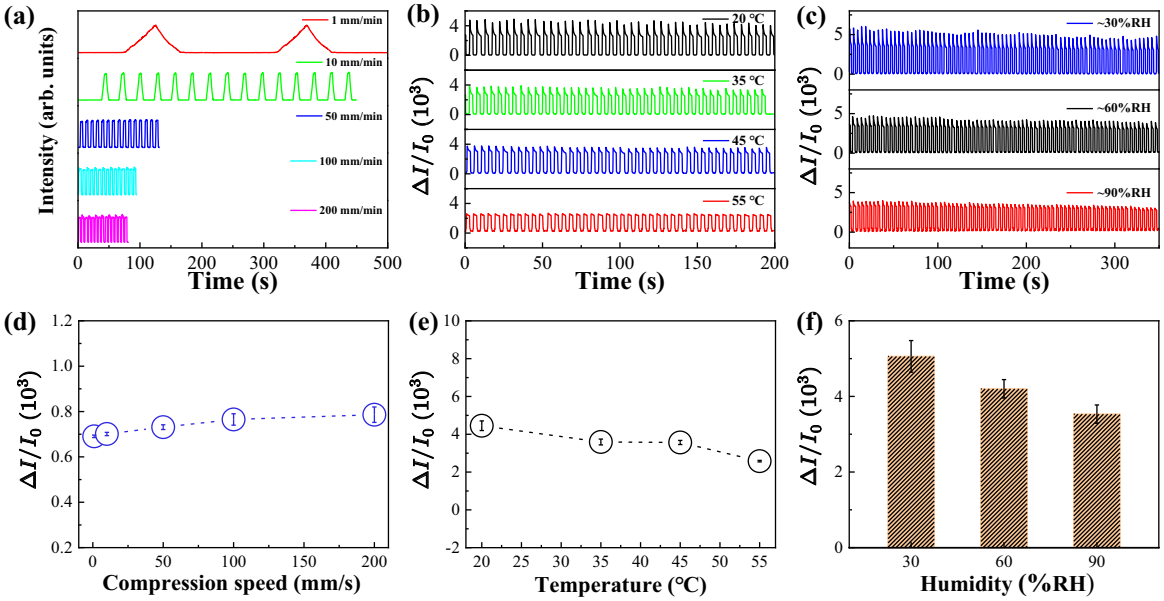

Fig. 3. Dynamic response and environmental adaptability of the PVA/GO/COOH-CNT composite-film sensor. (a) Real-time response signals of the sensor under different compression speeds of 1 mm·min^{-1}, 10 mm·min^{-1}, 50 mm·min^{-1}, 100 mm·min^{-1}, and 200 mm·min^{-1}. (b) Current responses of the sensor under different temperatures of 20 °C, 35 °C, 45 °C, and 55 °C. (c) Current responses of the sensor under different humidity conditions of approximately 30%, 60%, and 90% RH. (d) Statistical analysis of the normalized response under different compression speeds. (e) Statistical analysis of the normalized response under different temperatures. (f) Statistical analysis of the normalized response under different humidity conditions.

Figure 3(a) shows the real-time response signals of the sensor under different compression speeds of 1 mm·min^{-1}, 10 mm·min^{-1}, 50 mm·min^{-1}, 100 mm·min^{-1}, and 200 mm·min^{-1}. The sensor maintains clear and repeatable output signals at all tested compression speeds, indicating that the PVA/GO/COOH-CNT composite film can respond effectively to dynamic mechanical stimuli. As the compression speed increases, the signal frequency and waveform characteristics change accordingly, while the response remains distinguishable and stable. The statistical analysis in Fig. 3(d) further confirms that the sensor can maintain a reliable normalized response under different loading rates, demonstrating its adaptability to various dynamic pressure conditions.

The temperature-dependent sensing performance was evaluated at 20 °C, 35 °C, 45 °C, and 55 °C, as shown in Fig. 3(b). The normalized response varied gradually with increasing temperature. This behavior may be associated with enhanced segmental mobility and partial softening of the PVA matrix at elevated temperatures. Increased polymer-chain mobility may facilitate stress relaxation and modify the transfer of external pressure to the GO/COOH-CNT conductive network. Thermal expansion may also alter the distances and contact states between adjacent conductive components. These effects can influence the initial electrical resistance and reduce the incremental formation of conductive contacts during compression, resulting in a temperature-dependent variation in the normalized pressure response. Nevertheless, periodic and distinguishable pressure responses were retained throughout the investigated temperature range.

Humidity-dependent sensing performance was also investigated under relative humidity conditions of approximately 30%, 60%, and 90% RH, as shown in Fig. 3(c). The normalized response varied with increasing relative humidity. Both PVA and GO contain abundant hydrophilic hydroxyl and oxygen-containing functional groups that can adsorb water molecules under humid conditions. Water uptake may induce partial plasticization and swelling of the PVA matrix, alter the interlayer spacing of GO sheets, and modify interfacial contact

states within the PVA/GO/COOH-CNT composite network. These changes may influence the initial conductive pathways, CNT–CNT contact states, interfacial electrical resistance, and the magnitude of the pressure-induced electrical response. Despite the humidity-dependent variation in response amplitude, repeatable cyclic pressure signals were maintained over the investigated humidity range.

These results indicate that the sensor maintains distinguishable and repeatable pressure responses under different compression speeds, temperatures, and humidity conditions. However, the response magnitude is not completely independent of temperature and humidity. Therefore, environmental calibration or suitable encapsulation may be beneficial for quantitative sensing applications under strongly varying ambient conditions.

4.1. Wearable sensing applications

To demonstrate the practical potential of the PVA/GO/COOH-CNT composite-film sensor in wearable electronics, several human-signal monitoring tests were performed, as shown in Fig. 4. The sensor was attached to different positions of the human body to detect pressure or deformation signals generated by physiological activities and joint motions. During the tests, the output signal was recorded in real time under a constant-voltage mode.

Wrist-pulse monitoring was first carried out to evaluate the capability of the sensor to detect subtle physiological pressure signals. As shown in Fig. 4(a), the sensor was attached to the wrist near the radial artery for pulse-wave detection. The contact between the sensor and the skin enabled the pressure fluctuations induced by arterial pulsation to be converted into electrical signals. Figure 4(b) shows the real-time pulse signals recorded under different physiological states, including resting, slow walking, and brisk walking. The corresponding pulse rates were approximately 69 bpm, 102 bpm, and 106 bpm (beats per minute), respectively. The increase in pulse rate after walking indicates that the sensor can track physiological changes associated with different activity states. The enlarged pulse waveforms exhibit distinguishable characteristic peaks, suggesting that the sensor has sufficient sensitivity to capture weak arterial pulse-induced pressure fluctuations. These results demonstrate its potential for wearable cardiovascular signal monitoring.

The sensor was further used to monitor joint-motion signals. As shown in Fig. 4(c), the device was attached to a finger joint to detect finger-bending motions at different angles. When the finger was repeatedly bent and released, the sensor generated periodic response signals corresponding to joint deformation. The signal amplitude increased with the bending angle from 30° to 60° and 90°, indicating that larger deformation produced a stronger piezoresistive response. The distinguishable responses at different bending angles demonstrate that the sensor can effectively identify finger-motion states, showing potential for gesture recognition and human–machine interaction.

Figure 4(d) shows the monitoring of wrist-bending motions. The sensor produced repeatable response signals during cyclic wrist bending and releasing. The signal amplitude increased as the bending angle increased from 30° to 60°, confirming that the device can distinguish different wrist-motion states. The stable and angle-dependent output further indicates that the PVA/GO/COOH-CNT composite-film sensor can be used for dynamic joint-motion monitoring with good repeatability.

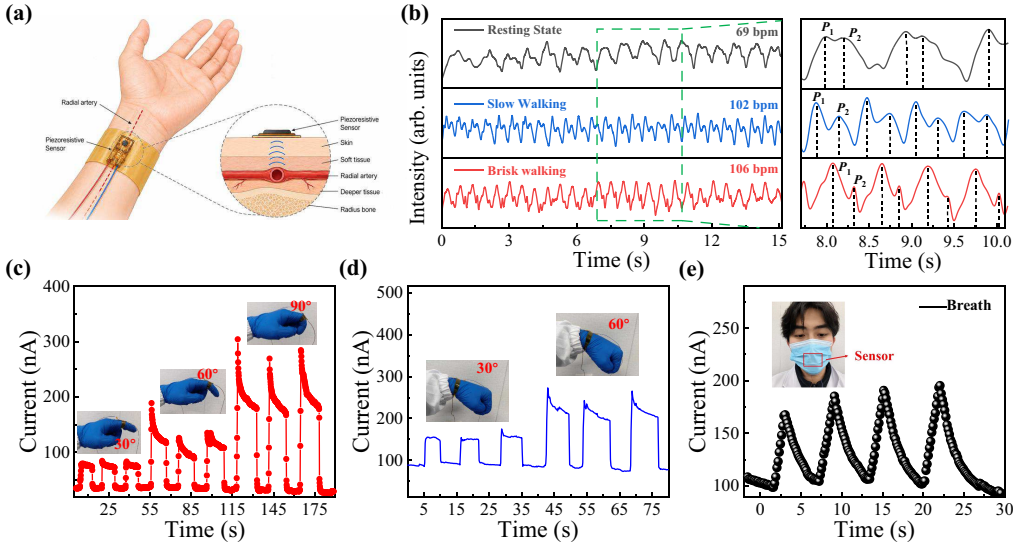

Fig. 4. Wearable sensing applications of the PVA/GO/COOH-CNT composite-film sensor. (a) Photograph and schematic illustration of the sensor attached to the wrist for radial artery pulse monitoring. (b) Real-time wrist-pulse signals recorded under resting, slow-walking, and brisk-walking states, with corresponding pulse rates of approximately 69 bpm, 102 bpm, and 106 bpm, respectively; enlarged waveforms show characteristic pulse peaks. (c) Real-time monitoring of finger-bending motions at different bending angles of 30°, 60°, and 90°. (d) Monitoring of wrist-bending motions at bending angles of 30° and 60°. (e) Respiration monitoring using the sensor mounted on a face mask.

In addition to pulse and joint-motion monitoring, respiration detection was also performed. As shown in Fig. 4(e), the sensor was mounted on a face mask near the mouth and nose region to detect airflow- or pressure-induced changes during breathing. The recorded signal displayed regular periodic peaks corresponding to respiration cycles. The stable waveform and distinguishable breathing pattern suggest that the sensor is capable of detecting low-amplitude physiological signals, indicating its potential for wearable respiratory monitoring. These wearable demonstrations confirm that the PVA/GO/COOH-CNT composite-film sensor can detect both subtle physiological signals and large-amplitude human motions. The ability to monitor wrist pulse, activity-dependent pulse variation, finger bending, wrist bending, and respiration highlights its promising potential for wearable health monitoring, motion recognition, and human–machine interaction.

4.2. Comparison with reported flexible piezoresistive pressure sensors

To further evaluate the sensing performance of the PVA/GO/COOH-CNT composite-film sensor, its key parameters were compared with those of previously reported flexible piezoresistive pressure sensors, as summarized in Table 1. The comparison includes material system, detection range, sensitivity, detection limit, response/recovery time, cycling stability, and representative application scenarios.

Table 1. Performance comparison of different flexible piezoresistive pressure sensors.

Material system	Detection range	Sensitivity	Detection limit	Response/recovery time	Cycling stability	Application scenarios	Ref.
GO/PPy@PU sponge	75 Pa–15 kPa	0.79 kPa^{-1}	75 Pa	$<$ 70 ms	$>$ 10000 cycles	Human motion detection	Ref. [36]
PI/rGO composite aerogel	0–59 kPa	1.33 kPa^{-1}	3 Pa	60/70 ms	$>$ 1000 cycles	Wrist pulse, blowing, finger bending, running	Ref. [37]
Graphene ink/lotus-leaf-inspired hierarchical structure	0–25 kPa	1.2 kPa^{-1}	Not specified	Not specified	Not specified	Wrist pulse, acoustic waves, pressure distribution imaging	Ref. [38]
CNT/PVA composite	0–400 kPa	0.1377 kPa^{-1} ($<$ 90 kPa)	Not specified	160 ms	$>$ 1200 cycles	Joint bending, muscle activity	Ref. [39]
PDMS/CNT–TPU/MXene	0–25 kPa	82.17 kPa^{-1}	Not specified	100/100 ms	$>$ 2000 cycles	Joint bending, gait monitoring, gesture recognition	Ref. [40]
MXene/PEO composite nanofiber membrane	0–500 kPa	44.34 kPa^{-1} (0–50 kPa); 12.99 kPa^{-1} (50–500 kPa)	Not specified	150/45 ms	$>$ 10000 cycles	Pulse monitoring, human health monitoring	Ref. [41]
PVA/GO/COOH-CNT	44.2 Pa–397.89 kPa	152.1 kPa^{-1}; 39.7 kPa^{-1}; 14.5 kPa^{-1}*	44.2 Pa	333/267 ms	$>$ 5000 cycles	Wrist pulse, finger bending, wrist bending, respiration monitoring	This work

*The three sensitivities for this work were obtained from linear fitting in the pressure ranges of 44.2 Pa–8.49 kPa, 8.49–84.07 kPa, and 84.07–309.73 kPa, respectively.

As shown in Table 1, the present sensor exhibits a broad pressure-response range from 44.2 Pa to 397.89 kPa and a low detection limit of 44.2 Pa. The normalized response shows three segmented sensitivity regions, with sensitivities of 152.1 kPa^{-1}, 39.7 kPa^{-1}, and 14.5 kPa^{-1} over the pressure ranges of 44.2 Pa–8.49 kPa, 8.49–84.07 kPa, and 84.07–309.73 kPa, respectively. Compared with reported GO-, CNT-, graphene-, and MXene-based piezoresistive sensors, the PVA/GO/COOH-CNT sensor demonstrates a balanced performance in terms of sensitivity, detection range, low-pressure detectability, response speed, and cyclic stability. In addition, the sensor was fabricated through a simple solution-processing and blade-coating method, which is beneficial for flexible device integration.

The present sensor also maintained stable output over more than 5000 loading–unloading cycles at approximately 4.42 kPa and was successfully applied to wrist-pulse monitoring, finger bending, wrist bending, and respiration detection. These comparisons indicate that the PVA/GO/COOH-CNT composite-film sensor has promising potential for wearable pressure sensing, human-motion recognition, and physiological signal monitoring.

5. Conclusion

In summary, a flexible piezoresistive pressure sensor based on a PVA/GO/COOH-CNT composite film was successfully developed via a facile solution-processing and blade-

coating strategy. The composite sensing film was prepared by dispersing COOH-CNTs in a GO aqueous dispersion, mixing with PVA solution to form a homogeneous composite ink, and fabricating the film by repeated blade coating and thermal drying. The sensor was assembled in a sandwich configuration using the PVA/GO/COOH-CNT composite film as the active sensing layer and Pt/PI films as the top and bottom electrodes.

The composite film exhibited a continuous surface morphology and a compact layered cross-section with a thickness of approximately 100 μm. In the composite structure, PVA provided the flexible film-forming matrix, GO sheets served as a layered framework, and COOH-CNTs acted as conductive bridges for pressure-induced resistance modulation. The sensor exhibited approximately linear current–voltage characteristics from −2 V to 2 V under applied pressures from 0 to 88.4 kPa, with R^2 values ranging from 0.98527 to 0.99289. The normalized current response exhibited three sensitivity regimes, with sensitivities of 152.1 kPa^{-1}, 39.7 kPa^{-1}, and 14.5 kPa^{-1} over the pressure ranges of 44.2 Pa–8.49 kPa, 8.49–84.07 kPa, and 84.07–309.73 kPa, respectively. The sensor also achieved a low detection limit of 44.2 Pa, a broad pressure-response capability up to 397.89 kPa, and response/recovery times of 333 ms and 267 ms, respectively, based on the 90% signal-change criterion.

In addition, the sensor maintained stable output over more than 5000 loading–unloading cycles at approximately 4.42 kPa, demonstrating good repeatability and cyclic durability. The device retained distinguishable and repeatable responses under different compression speeds, temperatures, and humidity conditions, although the response magnitude varied with environmental conditions. Wearable demonstrations further showed that the sensor could monitor wrist pulse, finger bending, wrist bending, and respiration signals, indicating its capability for detecting both subtle physiological signals and large-amplitude human motions. These results demonstrate that the PVA/GO/COOH-CNT composite-film sensor offers a promising material and device platform for flexible wearable pressure sensing, health monitoring, motion recognition, and human–machine interaction.

Acknowledgment

Project supported by the National Natural Science Foundation of China (Grant Nos. 12575041, 12504237, and 12405036).

References

[1] Chen Q, Akram W, Cao Y, Ge C, Lin T and Fang J 2023 *Carbon Neutral.* **2** 63
[2] Gao Y, Ota H, Schaler E W, Chen K, Zhao A, Gao W, Fahad H M, Leng Y, Zheng A, Xiong F, Zhang C, Tai L C, Zhao P, Fearing R S and Javey A 2017 *Adv. Mater.* **29** 1701985
[3] Khan Y, Ostfeld A E, Lochner C M, Pierre A and Arias A C 2016 *Adv. Mater.* **28** 4373
[4] Mohan V, Reji R P, Krishnamoorthy K, Sivalingam Y, Jayaraman S V and Kim S J 2025 *Carbon Neutral.* **4** e70038
[5] Rogers J A, Someya T and Huang Y 2010 *Science* **327** 1603
[6] Zarei M, Hoon Kim J, Tark Han J and Goo Lee S 2024 *Chem. Eng. J.* **479** 147849
[7] Zhao X F, Hang C Z, Lu H L, Xu K, Zhang H, Yang F, Ma R G, Wang J C and Zhang D W 2020 *Nano Energy* **68** 104346
[8] Tagawa Y, Lee S, Someya T and Yokota T 2023 *Adv. Electron. Mater.* **9** 2201304
[9] Liu Y F, Hu H Y, Li J Y, Wang H, Zhao Y, Wang J, Wu Y B, Li Y J, Zhang G Y, Sun Q Q, Zhu Y F, Tang R R, Wu X W, Wang J Z, Dou S X, Chou S L and Xiao Y 2024 *Sci. China Chem.* **67** 4242
[10] Chen W and Yan X 2020 *J. Mater. Sci. Technol.* **43** 175
[11] Zhang S, Sun K, Liu H, Chen X, Zheng Y, Shi X, Zhang D, Mi L, Liu C and Shen C 2020 *Chem. Eng. J.* **387** 124045
[12] Zhang B, Liu F, Chen S, Huang L, Zhong Y, Fan W and Li J 2025 *Chem. Eng. J.* **503** 158506
[13] Hou X, Zhong J, He J, Yang C, Yu J, Mei L, Mu J, Geng W and Chou X 2022 *Sci. China Technol. Sci.* **65** 1169
[14] Chen J, Chen K, Jin J, Wu K, Wang Y, Zhang J, Liu G and Sun J 2023 *Nano Lett.* **23** 11958
[15] Li Y, Dong M, Zou X, Zhang J, Zhang J and Huang X 2023 *Front. Phys.* **18** 63303
[16] Cui J, Nan X, Shao G and Sun H 2021 *Polymers* **13** 3465
[17] Kang S, Lee J, Lee S, Kim S, Kim J K, Algadi H, Al-Sayari S, Kim D E, Kim D and Lee T 2016 *Adv. Electron. Mater.* **2** 1600356
[18] Wu S, Zhang J, Ladani R B, Ravindran A R, Mouritz A P, Kinloch A J and Wang C H 2017 *ACS Appl. Mater. Interfaces* **9** 14207
[19] Pang Y, Tian H, Tao L, Li Y, Wang X, Deng N, Yang Y and Ren T L 2016 *ACS Appl. Mater. Interfaces* **8** 26458
[20] Tao K, Yi H, Yang Y, Chang H, Wu J, Tang L, Yang Z, Wang N, Hu L, Fu Y, Miao J and Yuan W 2020 *Nano Energy* **67** 104197
[21] Yue Y, Liu N, Ma Y, Wang S, Liu W, Luo C, Zhang H, Cheng F, Rao J, Hu X, Su J and Gao Y 2018 *ACS Nano* **12** 4224
[22] Cui X, Ruan Q, Zhuo X, Xia X, Hu J, Fu R, Li Y, Wang J and Xu H 2023 *Chem. Rev.* **123** 6891
[23] Shan G, Ding Z and Gogotsi Y 2023 *Front. Phys.* **18** 13604
[24] Cheng Y, Jiang B, Chaemchuen S, Verpoort F and Kou Z 2023 *Carbon Neutral.* **2** 213
[25] Liu H, Xu T, Cai C, Liu K, Liu W, Zhang M, Du H, Si C and Zhang K 2022 *Adv. Funct. Mater.* **32** 2113082
[26] Glamazda A Y, Stepanian S G, Karachevtsev M V, Plokhotnichenko A M, Adamowicz L and Karachevtsev V A 2020 *Physica E* **124** 114279
[27] Li W, Zhou T, Zhang Z, Li L, Lian W, Wang Y, Lu J, Yan J, Wang H, Wei L and Cheng Q 2024 *Science* **385** 62
[28] Cui X, Guo J, Araby S, Abbassi F, Zhang C, Diaby A and Meng Q 2022 *Nanotechnology* **33** 415701
[29] Secor E B, Gao T Z, Islam A E, Rao R, Wallace S G, Zhu J, Putz K W, Maruyama B and Hersam M C 2017 *Chem. Mater.* **29** 2332
[30] Wang Y and Wang Y 2024 *Carbon Neutral.* **3** 798
[31] Zhang C, McKeon L, Kremer M P, Park S H, Ronan O, Seral-Ascaso A, Barwich S, Coile'ain C 'O, McEvoy N, Nerl H C, Anasori B, Coleman J N, Gogotsi Y and Nicolosi V 2019 *Nat. Commun.* **10** 1795
[32] Gu M, Zhao B, Gao J, Zhou X, Huang L, Wang J, Wei L, Yang C and Chen M 2024 *Adv. Funct. Mater.* **34** 2400494
[33] Hu X, Zhao B, Tang Z, Wang L, Yang C and Chen M 2026 *Acta Phys. Sin.* **75** 100806 (in Chinese)
[34] Alamusi, Hu N, Fukunaga H, Atobe S, Liu Y and Li J 2011 *Sensors* **11** 10691
[35] Ren X and Seidel G D 2013 *J. Intell. Mater. Syst. Struct.* **24** 1459
[36] Lv B, Chen X and Liu C 2020 *Sensors* **20** 1219
[37] Xu Q, Chang X, Zhu Z, Xu L, Chen X, Luo L, Liu X and Qin J 2021 *RSC Adv.* **11** 11760
[38] Shi J, Wang L, Dai Z, Zhao L, Du M, Li H and Fang Y 2018 *Small* **14** 1800819
[39] Chen L, Huang Y, Ning H, Liu Y, Tang H, Zhou R, Jin S, Zheng J, Yao R and Peng J 2025 *Polymers* **17** 1378
[40] Wang M, Wang G, Zheng M, Liu L, Xu C, Liu Z and He L 2024 *J. Mater. Chem. A* **12** 22931
[41] Liu L C, Yuan Y, Xu H, Qin X K, Wang X F, Lou Z and Wang L L 2025 *J. Semicond.* **46** 042401